Design of a fiber-optic quasi-distributed strain sensors ring network based on a white-light interferometric multiplexing technique

Libo Yuan, Limin Zhou, Wei Jin, and Jun Yang

A fiber-optic quasi-distributed strain sensors ring network has been designed based on a Mach–Zehnder optical paths interrogator. The optical paths matching for each sensor are discussed, and the optical power budgetary analysis is performed. The relation between the number of sensors and the intensity of the signals of the ring network is given for evaluation of the multiplexing capacity. Experimentally, a seven-sensor array ring network was realized under the condition of light source power 35 μW at 1310 nm, and the distribution strain test was also demonstrated. © 2002 Optical Society of America

OCIS codes: 060.2370, 060.4230, 060.4250, 060.2430.

1. Introduction

In most distributed, fiber-optic sensing systems, sensors are fabricated or connected in one fiber line. Examples of these systems include fiber Bragg grating sensors,[1,2] optical time-domain reflectometer distributed sensors,[3,4] and white-light, distributed fiber-optic sensing systems in parallel and in series types.[5–7] However, there are still problems that have blocked the application of fiber-optic sensors in smart structures, especially in large-scale smart structures. They have one main drawback: if one sensor or if some point in the fiber line embedded in the smart structure breaks down because of local damage to the structure, then some part of or even the entire system fails. The perceived requirement for optical sensor networks, rather than for independent measuring devices, has stimulated the investigation of multiplexing and networking techniques for optical point sensors.[8,9]

White-light interferometry, as a technique employing low-coherence broadband light sources, has been a very active area of research in recent years. The idea of using a short-coherence-length source to separate the signals returning from a series of sensors was first published by Al-Chalabi *et al.*[10] Brooks *et al.*[11] proposed a series of Mach–Zehnder interferometers and a ladder-coherence multiplexing scheme. Valeria Gusmeroli[12] reported a low-coherence, polarimetric sensors array multiplexed on a fiber line. W. V. Sorin and D. M. Baney[13] and D. Inaudi *et al.*[14] further developed and simplified the quasi-distributed, low-coherence, fiber-optic sensor array based on the Michelson interferometer.

In our current work, a white-light, interferometric fiber-optic sensors ring network has been designed for measuring or monitoring large-scale, smart structure distribution strains. The technique uses a scanning Mach–Zehnder interferometer to determine the optical path changes of fiber-optic sensors from the bidirectional optical fiber ring. The technique can make absolute measurements with high resolution. The parameters that can be measured include position, displacement, strain, and temperature. One can configure white-light interferometers to perform quasi-distributed measurement by multiplexing a number of sensors onto the fiber ring. The sensors ring network not only satisfies the redundancy requirement of a practical sensing system but also provides a damage diagnosis methodology for large-scale smart structures.

2. Configuration of Fiber-Optic Sensors Ring Network

The white-light, interferometric, multiple-point sensor ring network topology is described in Fig. 1. It consists of a light-emitting diode (LED), a photodiode

L. Yuan (lbyuan@vip.sina.com) and J. Yang are with the Department of Physics, Harbin Engineering University, Harbin 15001, China. L. Yuan is also with and L. Zhou and W. Jin are with the Hong Kong Polytechnic University, Hong Kong, China. L. Yuan and L. Zhou are with the Department of Mechanical Engineering. W. Jin is with the Department of Electrical Engineering.

Fig. 1. Fiber-optic, white-light interferometric strain sensors ring network configuration.

Fig. 2. Optical path and reflective signals analysis diagram for the fiber-optic sensor $l_{j,j+1}$.

(PD) detector, a fiber-optic Mach–Zehnder optical path interrogator, and a series of fiber segments connected to one another to form a ring topology. The light is launched into the ring network sensing array by passing the imbalanced Mach–Zehnder interrogator optical paths and then reaches each fiber-optic sensor. The optical path difference (OPD) of the Mach–Zehnder interferometer can be varied through use of a scanning prism. The scanning prism is used to adjust the OPD of the Mach–Zehnder interferometer to match and trace the change of the fiber length in each sensing segment. We make the OPD of the Mach–Zehnder interferometer nearly equal to the fiber sensor gauge length, so that the two reflected light waves from both ends of the fiber sensor surface can match each other. When the OPD of the Mach–Zehnder interferometer is equal to the fiber sensor gauge length, a white-light fringe pattern is produced. The central fringe, which is located in the center of the fringe pattern and has the highest amplitude peak, corresponds to the unique fiber sensor. As the optical path of the fiber sensor is modulated by the ambient perturbation, for instance, strain or temperature, then the perturbation parameters related to the optical path change are measured and recorded by means of the interference signal peak shift.

In this sensing system the sensors consists of N sensing segments (N sensors) connected in series with partial reflectors between the adjacent sensors. The lengths of the sensing segments are chosen to be approximately equal to the OPD of the Mach–Zehnder interferometer. A moving, reflective prism opposite the twin gradient refractive-index (GRIN) lens and mounted on a step-motor-positioning system fine tunes the OPD of the Mach–Zehnder interferometer to match that of the sensors gauge lengths. Because this matching sets each individual sensor in a unique position, this multiplexing technique is classified as spatial-division multiplexing (SDM).

3. Measuring Principle

The multiplexed sensors ring network system is based on the basic measuring principle described in Section 1. Assuming that the gauge lengths of the fiber sensors are $l_{12}, l_{23}, \ldots, l_{N,N+1}$, respectively and
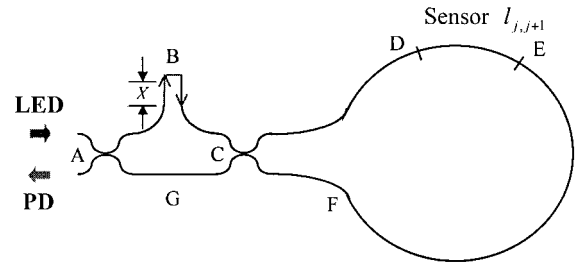
that the differential optical path of the Mach–Zehnder interrogator is fixed as shown in Fig. 1,

$$nL_{ABC} - nL_{AGC} = 2X + nL_0 \text{(OPD)} \qquad (1)$$

where X is the distance between the GRIN lens and the scanning prism.

For the fiber-optic sensor $l_{j,j+1}$, as shown in the equivalent optical path in Fig. 2, the all-reflective optical paths related with sensor $l_{j,j+1}$ are

$$2n(L_{ABC} + L_{CD}) + 4X_{j,j+1}, \qquad (2)$$

$$2n(L_{ABC} + L_{CD}) + 4X_{j,j+1} + 2nl_{j,j+1}, \qquad (3)$$

$$2n(L_{ABC} + L_{CFE}) + 4X_{j,j+1}, \qquad (4)$$

$$2n(L_{ABC} + L_{CFE}) + 4X_{j,j+1} + 2nl_{j,j+1}, \qquad (5)$$

$$2n(L_{AGC} + L_{CD}), \qquad (6)$$

$$2n(L_{AGC} + L_{CD}) + 2nl_{j,j+1}, \qquad (7)$$

$$2n(L_{AGC} + L_{CFE}), \qquad (8)$$

$$2n(L_{AGC} + L_{CFE}) + 2nl_{j,j+1}, \qquad (9)$$

$$n(L_{ABC} + L_{AGC} + 2L_{CD}) + 2X_{j,j+1}, \qquad (10)$$

$$n(L_{ABC} + L_{AGC} + 2L_{CD}) + 2X_{j,j+1} + 2nl_{j,j+1}, \qquad (11)$$

$$n(L_{ABC} + L_{AGC} + 2L_{CFE}) + 2X_{j,j+1}, \qquad (12)$$

$$n(L_{ABC} + L_{AGC} + 2L_{CFE}) + 2X_{j,j+1} + 2nl_{j,j+1}, \qquad (13)$$

$$n(L_{AGC} + L_{ABC} + 2L_{CD}) + 2X_{j,j+1}, \qquad (14)$$

$$n(L_{AGC} + L_{ABC} + 2L_{CD}) + 2X_{j,j+1} + 2nl_{j,j+1}, \qquad (15)$$

$$n(L_{AGC} + L_{ABC} + 2L_{CFE}) + 2X_{j,j+1}, \qquad (16)$$

$$n(L_{AGC} + L_{ABC} + 2L_{CFE}) + 2X_{j,j+1} + 2nl_{j,j+1}. \qquad (17)$$

Case 1. If the OPD of the Mach–Zehnder interrogator $L_0 \approx l_{\text{sens}}$ is chosen and adjusted $X_{j,j+1}$ over a small range, then paths (2) and (7) as well as paths (4) and (9) can match each other, and unwanted interference signals associated with nonadjacent reflectors and nonmatched reflectors lie outside the scan

range and are not detected. For this circumstance, we have

$$nL_0 + 2X_{j,j+1} = nl_{j,j+1}, \qquad j = 1, 2, \ldots, N. \quad (18)$$

In this way, one can measure the deformation of sensor $l_{j,j+1}$ by tracing the change of the prism-moving displacement $\Delta X_{j,j+1}$

$$\Delta(nl_{j,j+1}) = 2\Delta X_{j,j+1}. \quad (19)$$

Case 2. If OPD $L_0 \approx 2l_{\text{sens}}$ is chosen, then the matched paths are (2) with (11) and (15), (4) with (13) and (17), (7) with (10) and (14), and (8) with (12) and (16). The sum of the signals' intensity is much larger than that shown in case 1; thus we have

$$nL_0 + 2X_{j,j+1} = 2nl_{j,j+1}, \qquad j = 1, 2, \ldots, N. \quad (20)$$

4. Estimation of the Ring Network Maximum Multiplexable Sensor Number

A. Optical Signal Power Analysis

In the fiber-optic sensor array, a fraction of the optical source power is coupled into the fiber and distributed over the sensor array via several connectors. Each sensor element absorbs or diverts a certain amount of power (insertion loss), typically between 0.1 and 0.5 dB, which limits the maximum sensor number in the multiplexed sensing system.

We assume that the light source power is P_0; it is split by the first 3-dB coupler into two branches. One branch goes to the arm L_{ABC} of the Mach–Zehnder interrogator; as it passes through the GRIN lens and the prism, the power is $P_0\alpha_1\eta(X)/2$, where α and $\eta(X)$ represents the 3-dB coupler insertion loss parameter and insertion coupling function of the GRIN lens and scanning prism, respectively. Then the light is split by the second 3-dB coupler. In this branch the power coupled into one of the two legs of the sensor ring network is $P_0\alpha_1\alpha_2\eta(X)/4$. The clockwise light goes through lead fiber L_{CD} and, passing through $j - 1$ sensors, gets to sensor j. Meanwhile the counterclockwise light goes through L_{CFE} and, passing through $N - j$ sensors, reaches the same sensor j, where α_1 and α_2 represent the first and the second 3-dB coupler insertion loss parameters, respectively.

Similarly, the other branch goes along the arm L_{AGC} of the Mach–Zehnder interrogator, is directly divided by the second 3-dB coupler, and goes to sensor j from both direction of the sensor ring. The power injected into the sensor array for each of the two directions of the ring is $P_0\alpha_1\alpha_2/4$. It is larger then $P_0\alpha_1\alpha_2\eta(X)/4$ owing to few-decibel insertion losses of the GRIN lens and reflective prism coupling system. At each fiber sensor's end surface, the light wave is partly reflected and partly transmitted, as shown in Fig. 3.

To demonstrate this by calculation, assume that β_j represents the excess loss associated with sensor $l_{j,j+1}$ that is due to, for example, connection between the sensing segments. T_j and R_j, respectively, are
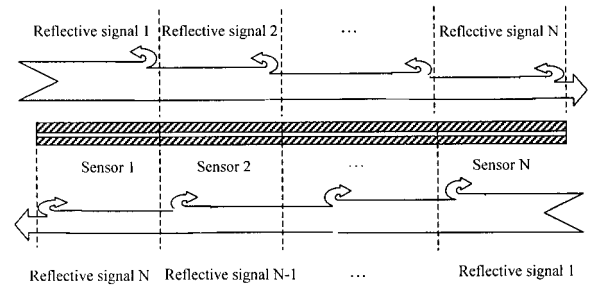

Fig. 3. Power fluxes of transmissive and reflective light signals in the sensors ring network.

the transmission and reflection coefficients of the jth partial reflector. T_j is in general smaller than $1 - R_j$ because of the loss factor β_j. The value $\eta(X_{j,j+1})$ is the loss associated with the prism and GRIN lenses systems and is a function of $X_{j,j+1}$. β_j', T_j', and R_j' represent, respectively, the loss, the transmission, and the reflection from the opposite direction as shown in Fig. 4.

Then the reflected light signal power arriving at the detector of sensor $l_{j,j+1}$ can be calculated as follows:

Case 1. For the condition $L_0 \approx l_{\text{sens}}$, the clockwise paths (2) and (7) match; the counterclockwise paths (4) and (9) match; thus the light wave signal following path (2) and the returned power may be given by

$$P_{CW2}(j) = \frac{P_0}{16} \alpha_1^2 \alpha_2^2 \eta^2(X_{j,j+1}) R_j \left\{ \prod_{k=1}^{j-1} T_k \beta_k \right\} \left\{ \prod_{k=1}^{j-1} T_k' \beta_k' \right\},$$
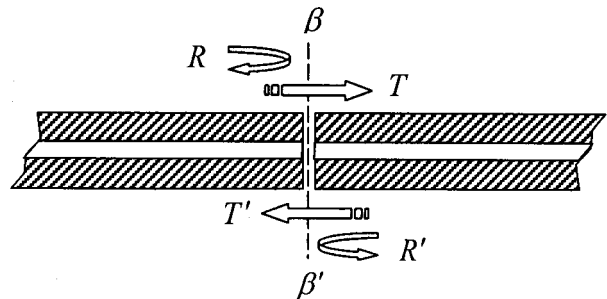$$j = 1, 2, \ldots, N + 1. \quad (21)$$

The light wave signal following path (7) and the returned power is

$$P_{CW7}(j+1) = \frac{P_0}{16} \alpha_1^2 \alpha_2^2 \eta^2(X_{j,j+1}) R_{j+1} \left\{ \prod_{k=1}^{j} T_k \beta_k \right\}$$
$$\times \left\{ \prod_{k=1}^{j} T_k' \beta_k' \right\},$$
$$j = 1, 2, \ldots, N + 1. \quad (22)$$

Fig. 4. Relation between the coefficients R, β, and T and R', β', and T' in the connection part of the adjacent sensors.

For counterclockwise paths (4) and (9), the detected optical signals power are

$$P_{CCW4}(j+1) = \frac{P_0}{16}\,\alpha_1{}^2\alpha_2{}^2\eta^2(X_{j,j+1})\,R'_{j+1}\left\{\prod_{k=j+2}^{N+1} T_k{}'\beta_k{}'\right\}$$

$$\times\left\{\prod_{k=j+2}^{N+1} T_k\beta_k\right\},$$

$$j = 1, 2, \ldots, N+1, \tag{23}$$

$$P_{CCW9}(j) = \frac{P_0}{16}\,\alpha_1{}^2\alpha_2{}^2 R_j{}'\left\{\prod_{k=j+1}^{N+1} T_k{}'\beta_k{}'\right\}\left\{\prod_{k=j+1}^{N+1} T_k\beta_k\right\},$$

$$j = 1, 2, \ldots, N+1. \tag{24}$$

The output signal power of sensor $l_{j,j+1}$ is proportional to the coherent mixing terms of the reflected light signals from the sensor's two matching paths, i.e.,

$$P_D(j, j+1) = 2[P_{CW2}(j)P_{CW7}(j+1)]^{1/2} + 2[P_{CCW4}(j+1)P_{CCW9}(j)]^{1/2}$$

$$= \frac{P_0}{8}\,\alpha_1{}^2\alpha_2{}^2\eta(X_{j,j+1})$$

$$\times\left\{(R_jR_{j+1}T_j\beta_jT_j{}'\beta_j{}')^{1/2}\left(\prod_{k=1}^{j-1} T_k\beta_k\right)\right.$$

$$\times\left(\prod_{k=1}^{j-1} T_k{}'\beta_k{}'\right)$$

$$+ (R_j{}'R'_{j+1}T_{j+1}\beta_{j+1}T'_{j+1}\beta'_{j+1})^{1/2}$$

$$\left.\times\left(\prod_{k=j+2}^{N+1} T_k\beta_k\right)\left(\prod_{k=j+2}^{N+1} T_k{}'\beta_k{}'\right)\right\}. \tag{25}$$

Case 2. For the condition $L_0 \approx 2l_{\text{sens}}$, the matched paths are (2) with (11) and (15); (4) with (13) and (17); (7) with (10) and (14); and (8) with (12) and (16). The procedure is similar to case 1 of this section; the sum of the coherent mixing terms of the reflected light signals can be calculated as

$$P_D(j, j+1) = 2\{P_{CW2}(j)[P_{CW11}(j+1) + P_{CW15}(j+1)]\}^{1/2} + 2\{P_{CCW4}(j+1)[P_{CCW13}(j) + P_{CW17}(j)]\}^{1/2}$$

$$= 2\{P_{CW7}(j+1)[P_{CW10}(j) + P_{CW14}(j)]\}^{1/2} + 2\{P_{CCW9}(j+1)$$

$$\times [P_{CCW12}(j) + P_{CCW16}(j)]\}^{1/2}$$

$$= \frac{P_0}{8}\,\alpha_1{}^2\alpha_2{}^2[2\eta(X_{j,j+1})]^{1/2}[1 + \eta(X_{j,j+1})]$$

$$\times\left\{(R_jR_{j+1}T_j\beta_jT_j{}'\beta_j{}')^{1/2}\left(\prod_{k=1}^{j-1} T_k\beta_k\right)\right.$$

$$\times\left(\prod_{k=1}^{j-1} T_k{}'\beta_k{}'\right)$$

$$+ (R_j{}'R'_{j+1}T_{j+1}\beta_{j+1}T'_{j+1}\beta'_{j+1})^{1/2}$$

$$\left.\times\left(\prod_{k=j+1}^{N+1} T_k\beta_k\right)\left(\prod_{k=j+1}^{N+1} T_k{}'\beta_k{}'\right)\right\}. \tag{26}$$
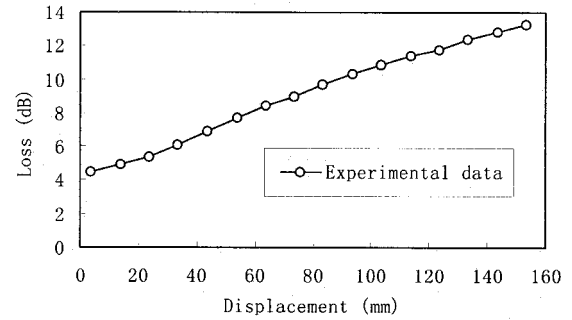

Fig. 5. Insertion coupling loss of GRIN lenses and prism versus the displacement X.

B. Maximum Number of the Multiplexable Sensor

If the detecting limit of the photodiode is $P_{\min}$, then, the maximum number of the total fiber-optic sensors can be evaluated by the condition

$$P_D(j, j+1) \geq P_{\min}. \tag{27}$$

To simplify the calculation, we assume that

$$R_j = R_j{}',$$
$$T_j = T_j{}',$$
$$\beta_j = \beta_j{}' \tag{28}$$

and that the coupler parameter $\alpha_1 \approx \alpha_2 = 0.98$ corresponds to the typically 3-dB coupler excess insertion loss 0.06 dB. The typical fiber-optic butt-connection insertion loss coefficient is chosen as $\beta_j = \beta_j{}' = 0.9$ $(j = 1, 2, \ldots, N+1)$. Under the condition of perpendicular incidence, the reflectivity at the fiber end surface is given by the Fresnel formula $R = (n-1)^2/(n+1)^2$. Where n is the index of the fiber core, the typical value is 1.46, corresponding to 4% reflectivity. For good butt-connected fiber ends, the air gap is smaller than the wavelength; in that case the typically reflectivity $R_j = R_j{}'$ is nearly equal to 1%. Therefore the transmission coefficient can be calculated as $T_j = T_j{}' = 0.89$. The measuring experimental data of the insertion coupling loss between GRIN lenses and prism versus the displacement X is shown in Fig. 5. We use the 6-dB average attenuation of the prism moving from 3 to 60 mm instead of the function $\eta(X_{j,j+1})$ to approximate the signal intensity, i.e. $\eta(X_{j,j+1}) = 1/4$. Then, the normalized optical signal power versus the fiber optic sensor number is plotted in Fig. 6.

To estimate the number of sensors that can be multiplexed with the proposed topology, first we assume that the minimum power that can be detected by the photodiode is $P_{\min}$. In a fiber-optic sensing system the typical detecting capability of the photodiode is ~ 1 nW. Taking into account the noise floor and other stray signals from the system, a reasonable detect limit is assumed to be $P_{\min} = 10$ nW. Second, the multiplexable number is different in cases 1 and 2 of this section. We use the ratio of Eq. (26) divided
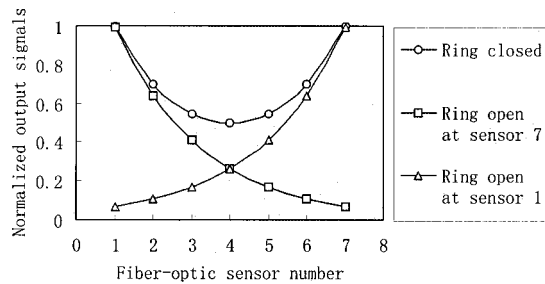
Fig. 6. Simulation results of normalized output signals of a seven-sensor fiber-optic ring network.

Fig. 8. Simulation results of relation between sensor number and its signal power level for a ring network system of a different size.

by Eq. (25) to compare the multiplexing capacities of the two cases:

$$\frac{P_D(j, j+1)|_{\text{Case 2}}}{P_D(j, j+1)|_{\text{Case 1}}} = \frac{[2\eta(X_{j,j+1})]^{1/2}[1 + \eta(X_{j,j+1})]}{\eta(X_{j,j+1})}.$$

$$(29)$$

For the prism–GRIN lens, a coupling loss of 4–10 dB corresponds to an $\eta(X_{j,j+1})$ change of 0.4–0.125. The ratio given by Eq. (29) is plotted as Fig. 7. This means that the multiplexing capacity of case 2 is much better than case 1.

With condition (27) and taking account of the above data for light source power $P_0 = 35$ µW, one can calculate the maximum number of the fiber sensors as $N_{\max} = 7$ in case 2 and $N_{\max} = 1$ in case 1, as shown in Fig. 8, whereas for light source power $P_0 = 3$ mW, we get $N_{\max} = 27$ in case 2 and $N_{\max} = 21$ in case 1.

The maximum sensor number may be limited by other factors, e.g., the available moving range of the scanning prism. In addition, the receiver noise floor, and hence the detecting sensitivity, would be a function of detector bandwidth, which depends on the required response time of the system and the scanning speed of the moving prism. For a specific system, a detailed analysis considering all these aspects is needed to fully assess the multiplexing capacity of the topology.

5. Experimental Results

A seven-sensor ring network was demonstrated in our experiments; the output signals corresponding to the seven white-light interferometric peaks are plot-
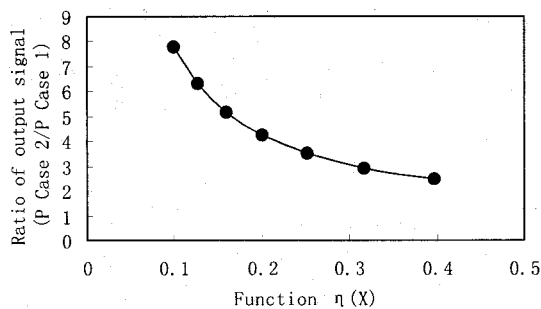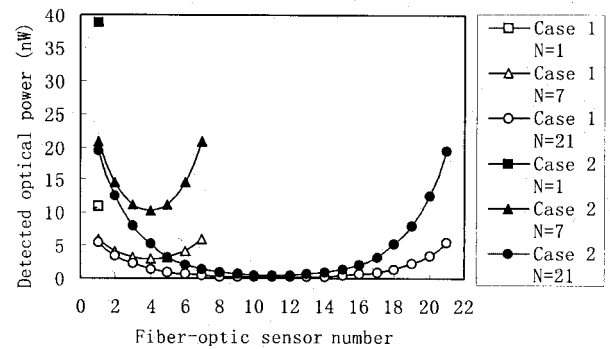
ted in Fig. 9. In the sensing ring network, the LED light source power is 35 µW at the center wavelength 1310 µm; the insertion loss of the GRIN lens–prism scanning system is from 4 to 8 dB in the scanning range of 3–60 mm. Each sensor's gauge length is ~100 mm. The OPD is selected at nearly twice the sensor gauge length (~200 mm), and we set that as

$$l_{78}(\text{Sensor 7}) > l_{67}(\text{Sensor 6}) > l_{56}(\text{Sensor 5})$$
$$> l_{45}(\text{Sensor 4}) > l_{34}(\text{Sensor 3})$$
$$> l_{23}(\text{Sensor 2}) > l_{12}(\text{Sensor 1}). \quad (30)$$

Figure 9 shows the sensor length order to be the same as that in our arrangement. The signals' power level is also approximately in agreement with our theoretical prediction, except for that of sensor 7. In our experimental results, it is shown that the signal power level of sensor 6 is higher than that of sensor 7 and differs from the theoretical estimation $I_{78} > I_{67}$. In fact, it is very difficult to ensure that each butt-connecting reflectivity has the same value.

To demonstrate the applicability of the system in real distributed deformation or strain measurements, we applied strains on the third, fifth, and seventh fiber-optic sensors, and left the other four sensors in a strain-free state. The testing results are plotted in Fig. 10, where it is shown that the fiber-optic sensors connected in the fiber ring can map the applied strain conditions, whereas the four strain-free sensors are not perturbed, and their in-
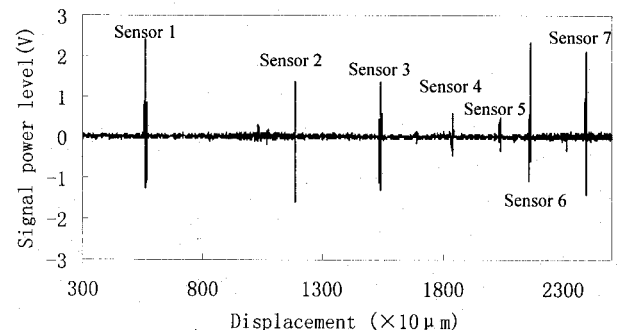

Fig. 7. Multiplexable comparison of cases 2 and 1.

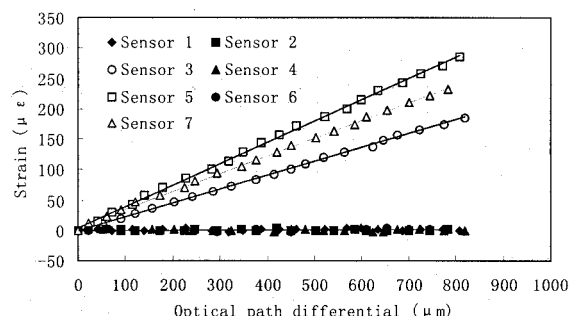

Fig. 9. Fiber-optic sensors' output signals power level.

Fig. 10. Distributed strain measurement results.

terference pattern peak positions have almost no shift. The resolution of the strain-sensing system is 5 $\mu\varepsilon$ for the current 100-mm fiber gauge-length case, and the measuring accuracy is 10 $\mu\varepsilon$.

6. Polarization Effect

It should be mentioned that the output signals of the sensors ring depend on the polarization states. Figure 11 shows the variation of the signals and the accompanying noise when the polarization controller in the ring (see Fig. 1) was adjusted. This variation occurs because the parts of the light signals that are not reflected at the partial reflectors (transmitted) mix coherently at the ring coupler as they travel through the optical path length. When the counter-propagating (transmitted) light signals are of the same polarization states, the light signal at the output port of the ring approaches zero owing to destructive interference.[15] When the counterpropagating signals are of different polarizations, the orthogonal polarization components increase in intensity and result in noise. Additionally, as the deformation varies in each sensor gauge length, starting with the first sensor, it changes the state of polarization. In this case, the multisensing capability would be reduced. It may therefore be necessary to control the polarization states to achieve optimal results. One method is by way of inserting a depolarizer between the LED light source and the first 3-dB coupler; the other solution is to use polarization-maintaining fibers in the sensing system to overcome the instability of the polarization state.
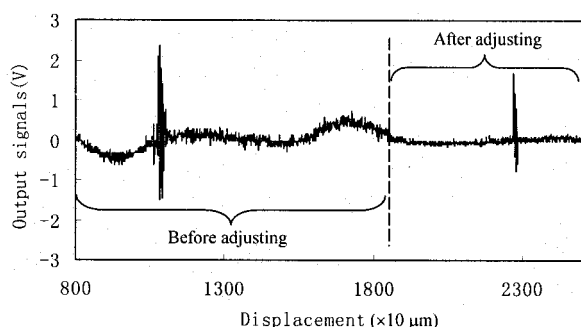

Fig. 11. Noise amplitude that is reduced greatly because the polarization state has been adjusted.

7. Conclusion

In conclusion, a multiplexed, fiber-optic deformation sensor ring network suitable for smart structure applications has been designed and demonstrated. The sensor system is based on a white-light, interferometric, Mach–Zehnder optical path interferometer technique. It is clear that multiplexed sensors ring network topology suffers from relatively large fiber-segment-induced optical reflective and excess insertion losses that generally limit the total number of sensors that can be accommodated in this configuration. However, it has been predicted that as many as 27 sensors can be operated on the ring topology when a 3-mW light source is used. In addition, this ring network architecture greatly improves the reliability of the system and provides a redundancy owing its bidirectional interrogation of the sensor ring. It means that even if at some point the sensor ring breaks down, the system will still work in the series of the fiber-optic sensor lines.

References

1. A. D. Kersey and W. W. Morey, "Multiplexed Bragg grating fiber-laser strain-sensor system with mode-locked interrogation," Electron. Lett. **29,** 112–114 (1993).
2. G. Duck and M. M. Ohn, "Distributed Bragg grating sensing with a direct group-delay measurement technique," Opt. Lett. **25,** 90–92 (2000).
3. E. Sensfelder, J. Burck, and H. J. Ache, "Characterization of a fiber-optic system for the distributed measurement of leakages in tanks and pipelines," Appl. Spectrosc. **52,** 1283–1298 (1998).
4. V. Lecoeuche, D. J. Webb, C. N. Pannell, and D. A. Jackson, "25 km Brillouin based single-ended distributed fibre sensor for threshold detection of temperature or strain," Opt. Commun. **168,** 95–102 (1999).
5. L. B. Yuan and F. Ansari, "White light interferometric fiber-optic distributed strain-sensing system," Sens. Actuators A **63,** 177–181 (1997).
6. L. B. Yuan and L. Zhou, "1 × N star coupler as a distributed fiber-optic strain sensor in a white-light interferometer," Appl. Opt. **37,** 4168–4172 (1998).
7. L. B. Yuan, L. Zhou, and W. Jin, "Quasi-distributed strain sensing with white-light interferometry: a novel approach," Opt. Lett. **25,** 1074–1076 (2000).
8. J. M. Senior, S. E. Moss, and S. D. Cusworth, "Wavelength division multiplexed optical point-sensor networks using injection laser diode sources," Opt. Laser Technol. **28,** 1–5 (1996).
9. W. Ecke, I. Latka, R. Willsch, A. Reutlinger, and R. Graue, "Fibre optic sensor network for spacecraft health monitoring," Meas. Sci. Technol. **12,** 974–980 (2001).
10. S. A. Al-Chalabi, B. Culshaw, and D. E. N. Davies, "Partially coherent sources in interferometry," in *Proceedings of 1st International Conference on Optical Fiber Sensors* IEE Conf. Pub. **221,** 132–135 (1983).
11. J. L. Brooks, R. H. Wentworth, R. C. Youngquist, M. Tur, B. Y. Kim, and H. J. Shaw, "Coherence multiplexing of fiber-optic interferometric sensors," J. Lightwave Technol. **LT-3,** 1062–1072 (1985).

12. V. Gusmeroli, "High-performance serial array of coherence multiplexed interferometric fiber-optic sensors," J. Lightwave Technol. **11,** 1681–1686 (1993).

13. W. V. Sorin and D. M. Baney, "Multiplexing sensing using optical low-coherence reflectometry," IEEE Photon. Technol. Lett. **7,** 917–919 (1995).

14. D. Inaudi, S. Vurpillot, and S. Lloret, "In-line coherence multiplexing of displacement sensors: a fiber optic extensometer," in *Smart Structures and Materials 1996: Smart Sensing, Processing, and Instrumentation*, K. A. Murphy and D. R. Huston, eds., Proc. SPIE **2178,** 251–257 (1996).

15. W. Jin, "Fiber optic gyroscope," in *Guided Wave Optical Sensors*, W. Jin, Y. Liao, and Z. Zhang, eds. (Science, Beijing, pp. 148–176 (1998).